

Accuracy of numerical relativity waveforms with respect to space-based gravitational wave detectors

Zun Wang,^{1,2} Junjie Zhao,^{1,2} and Zhoujian Cao ^{*1,2,3,†}

¹*Institute for Frontiers in Astronomy and Astrophysics,
Beijing Normal University, Beijing 102206, China*

²*Department of Astronomy, Beijing Normal University, Beijing 100875, China*

³*School of Fundamental Physics and Mathematical Sciences,
Hangzhou Institute for Advanced Study, UCAS, Hangzhou 310024, China*

The same to laser interferometer gravitational-wave observatory (LIGO), matched filtering technique will be critical to data analysis of gravitational wave detection by space-based detectors including LISA, Taiji and Tianqin. Waveform templates are basis for such matched filtering technique. In order to construct ready-to-use waveform templates, numerical relativity waveforms are start point. So the accuracy issue of numerical relativity waveforms is critically important. There are many investigations about this issue with respect to LIGO. But unfortunately there are few results on this issue with respect to space-based detectors. The current paper investigates this problem. Our results indicate that the existing numerical relativity waveforms are as accurate as 99% with respect to space-based detectors including LISA, Taiji and Tianqin. Such accuracy level is comparable to the one with respect to LIGO.

I. INTRODUCTION

Since the first successful detection of gravitational waves in 2015, about 100 gravitational wave events have been reported. All these events are found by matched filtering technique. Till now matched filtering technique is still the standard data analysis trick for gravitational waves detection [1, 2]. As expected, the situation will be also true for space-based detectors in the near future [3, 4].

In order to let the matched filtering technique work, accurate and complete waveform templates are needed [5–8]. Besides the above mentioned matched filtering method, there is time-frequency excess power identification method [9]. But if accurate waveform is available and aid the analysis, the method will become more efficient [10]. In addition, machine learning method is a new trick to treat gravitational wave data [11–16]. A data set consisting a large amount of gravitational wave samples is critical important to let the machine learning method work well. Since the real gravitational wave events are too few to play the role of such a data set, accurate waveform templates are needed. In a short summary, no matter what kind of data analysis means are taken, waveform templates are very important to gravitational wave data analysis.

A waveform template means the accurate waveform with respect to time or frequency when a set of source parameters are specified. That is to say a waveform template is valid only for a class of source falling in a specified parameters range. Till now gravitational wave astronomy community only understand binary compact object systems well. Consequently only waveform template of

binary systems is available currently. This fact also explains to some extent why only events of coalescence of binary objects are observed till now. In contrast, current detection ability for supernovae gravitational waves is quite weak [17]. Roughly the detection horizon is just 1kpc (Fig. 5(a) of [17]). The partial reason for such fact is the lack of accurate waveform template for supernovae gravitational waves.

Before the breakthrough of numerical relativity [18–22], the waveform template problem is treated mainly through post-Newtonian approximation [23]. As an enhanced post-Newtonian approximation method, effective one body theory shows better convergent behavior [24]. After the success of numerical relativity simulation of binary black hole merger, the complete inspiral-merger-ringdown behavior is revealed. The power of effective one body theory to describe the waveform of coalescence of binary object is verified [25]. After that the numerical relativity waveforms are extensively used to construct waveform templates for coalescence of binary objects.

Till now, there are a bundle of waveform templates for coalescence of binary objects available in the LIGO data analysis software. Among kinds of waveform template models including EOBNR series [26–31], IMRphenom series [32, 33], numerical relativity surrogate models [34–36] and others, the numerical relativity waveforms are bases for the waveform templates construction. When people talk about the accuracy of a waveform model, the numerical relativity waveforms are treated as the standard answer. So the accuracy of numerical relativity waveforms themselves are critically important to waveform template construction.

Both ground-based and space-based gravitational wave detectors utilize matched filtering techniques for detecting gravitational waves. Therefore, when calculating the accuracy of the templates, the formulas used are very similar to those of the matched filtering technique. Considering the detector noise is crucial when using the

*corresponding author

†Zhoujian Cao: zjcao@amt.ac.cn

matched filtering technique to search for signals. Hence, when calculating the accuracy of the waveform templates, it is necessary to take into account the sensitivity of different detectors. The noise characteristics of space-based gravitational wave detectors differ significantly from those of ground-based detectors. Therefore, the purpose of this article is to investigate whether the numerical relativity waveform's accuracy can meet the requirement of space-based detectors. When one discusses the accuracy of a waveform model, a specific detector should be referred. The accuracy issue of numerical relativity waveforms has been extensively studied against advanced LIGO detectors [37]. But this issue has not been investigated against space-based detectors. The current paper aims to do such an investigation and lays down a foundation of waveform template construction for space-based detectors.

In the next section we introduce the waveform accuracy estimation method. After that we apply the method in Sec. III to calculate waveform accuracy of the waveforms of SXS numerical relativity catalog. LISA, Taiji and Tianqin detectors are all considered. Finally the summary and conclusion are given in the last section.

II. MATCHING FACTOR AND ACCURACY INDICATOR

Following the idea of matched filtering data analysis trick, matching factor has been extensively used to quantify how close between two given waveforms. With respect to a detector sensitivity $S(f)$ which describes the one sided power spectrum of the detector noise, the matching factor of two real waveforms $h_1(t)$ and $h_2(t)$ can be expressed as

$$\text{FF} \equiv \max_t \frac{\langle h_1 | h_2 \rangle}{\|h_1\| \cdot \|h_2\|}, \quad (1)$$

$$\langle h_1 | h_2 \rangle = 2 \int_{f_{\text{low}}}^{f_{\text{up}}} \frac{\tilde{h}_1 \tilde{h}_2^* + \tilde{h}_1^* \tilde{h}_2}{S(f)} df, \quad (2)$$

$$\|h\| \equiv \sqrt{\langle h | h \rangle}, \quad (3)$$

where the “ $\tilde{(\cdot)}$ ” means the Fourier transformation, the “ $*$ ” means taking the complex conjugate, and the maximum is taken with respect to the time shift to align the two waveforms. $(f_{\text{low}}, f_{\text{up}})$ corresponds to the frequency band where the two waveforms should be compared. Within PyCBC software [38], the command line ‘pycbc.filter.matchedfilter.match’ can be used to do the above calculation of the matching factor FF. Together with the value of the matching factor, the time shift is also returned by the command line.

For a theoretical waveform template, two polarization waveforms will be given $h_+(t)$ and $h_\times(t)$. Usually people are used to the complex waveform defined as

$$h \equiv h_+ - ih_\times. \quad (4)$$

Then similar matching factor to (1) can be defined to quantify the closeness between two complex waveforms. The only difference to (1) is the maximum should be taken with respect to the initial phase besides the shifted time. The initial phase describes the phase difference between the two polarization modes $h_+(t)$ and $h_\times(t)$ at the initial time.

Assume we have two complex waveforms $h_{1,2} = h_{1,2+} - ih_{1,2\times}$, the linearity of inner product (2) results in

$$\begin{aligned} \langle h_1 | h_2 \rangle &= \langle h_{1+} | h_{2+} \rangle + \langle h_{1\times} | h_{2\times} \rangle \\ &\quad - i \langle h_{1+} | h_{2\times} \rangle - i \langle h_{1\times} | h_{2+} \rangle. \end{aligned} \quad (5)$$

In the mean time Eq. (2) can be equivalently expressed as

$$\langle h_1 | h_2 \rangle = 4\Re \int \frac{\tilde{h}_1 \tilde{h}_2^*}{S(f)} df, \quad (6)$$

where \Re means taking the real part. So we have

$$\langle h_1 | h_2 \rangle = \langle h_{1+} | h_{2+} \rangle + \langle h_{1\times} | h_{2\times} \rangle, \quad (7)$$

which corresponds to

$$\max_{t, \phi} \langle h_1 | h_2 \rangle = \max_{t_+} \langle h_{1+} | h_{2+} \rangle + \max_{t_\times} \langle h_{1\times} | h_{2\times} \rangle. \quad (8)$$

Here t means the time shift for the complex waveform, ϕ means the initial phase difference of the two polarization modes, and $t_{+, \times}$ are the time shifts for the two polarization waveforms. Due to the above relations, we have

$$\text{FF} = \frac{\text{FF}_+ \|h_{1+}\| \cdot \|h_{2+}\| + \text{FF}_\times \|h_{1\times}\| \cdot \|h_{2\times}\|}{\|h_1\| \cdot \|h_2\|}, \quad (9)$$

$$\text{FF}_+ \equiv \max_t \frac{\langle h_{1+} | h_{2+} \rangle}{\|h_{1+}\| \cdot \|h_{2+}\|}, \quad (10)$$

$$\text{FF}_\times \equiv \max_t \frac{\langle h_{1\times} | h_{2\times} \rangle}{\|h_{1\times}\| \cdot \|h_{2\times}\|}. \quad (11)$$

That is to say we can calculate the matching factors FF_+ and FF_\times for two polarization modes individually, then use the above equation to combine the final matching factor we wanted. In the current work we follow this way and use PyCBC tool to calculate the matching factor.

Similar to any other computing science topics, the only errors involved in numerical relativity include truncation errors and round off errors. Truncation errors are due to the numerical approximation of derivatives. Round off errors are due to the memory limit of computers. In practice, one needs to make sure the real calculation dominated by truncation errors. Consequently the final error related to the numerical solution is proportional to some power of the resolution used in the numerical calculation. The power index is nothing but the convergence order of the involved numerical algorithm. So we can use the difference between the results of two different resolutions to quantitatively estimate the error of the numerical solution.

In the current work we use the matching factor between the two numerical relativity waveforms of two different resolutions to quantify the accuracy of the numerical relativity waveforms. Specifically to the SXS waveform catalogs [37, 39], the finest and second finest resolutions are used.

III. ACCURACY OF NUMERICAL RELATIVITY WAVEFORMS

A. Fourier transforms of numerical relativity waveforms

Numerical relativity (NR) waveforms are presented in time domain. In order to calculate the matching factor explained in the last section, we need transform these waveforms to frequency domain. In practice, we use fast Fourier transformation to get the waveforms in frequency domain.

In order to reduce the Gibbs effect and spectral leakage resulting from truncation in the time domain, we apply the Plank window $\sigma_T(t)$ to the time domain waveform before the Fourier transformation. The Plank window $\sigma_T(t)$ is set as [40, 41]

$$\sigma(t) = \begin{cases} 0, & t < t_1 \\ \sigma_{start}(t), & t_1 \leq t < t_2 \\ 1, & t_2 \leq t < t_3 \\ \sigma_{end}(t), & t_3 \leq t < t_4 \\ 0, & t_4 \leq t \end{cases} \quad (12)$$

where σ_{start} is the segment that smoothly increases from 0 to 1 between t_1 and t_2 , and σ_{end} is the segment that smoothly decreases from 1 to 0 between t_3 and t_4 :

$$\begin{aligned} \sigma_{start}(t) &= \left[\exp\left(\frac{t_2-t_1}{t-t_1} + \frac{t_2-t_1}{t-t_2}\right) + 1 \right]^{-1}, \\ \sigma_{end}(t) &= \left[\exp\left(\frac{t_3-t_4}{t-t_3} + \frac{t_3-t_4}{t-t_4}\right) + 1 \right]^{-1}. \end{aligned} \quad (13)$$

Then, We further zero pad the waveform to the nearest power of 2.

B. Frequency range of numerical relativity waveforms

Typically we get waveforms in frequency domain like the one shown in Fig. 1. Apparently only the part between the two vertical dash lines is reliable. The left vertical line corresponds to the lowest frequency f_{min} of the numerical relativity waveform which is determined by the length of the waveform. The right vertical line corresponds to the highest frequency f_{max} where the numerical error begins to dominate.

There are 1872 waveforms in the SXS catalog [39] who have more than one resolution result. In Fig. 2(a) and (b) we plot Mf_{min} and Mf_{max} of these waveforms. Here M

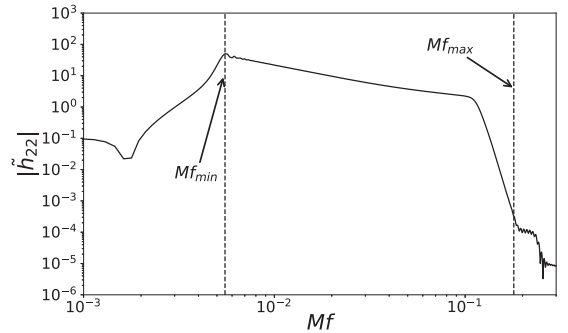


FIG. 1: Frequency waveform of SXS:BBH:2106. This waveform corresponds to a quasi-circular coalescing binary black hole system with mass ratio 1, dimensionless spin $\vec{\chi}_1 = (0, 0, 0.8998)$ and $\vec{\chi}_2 = (0, 0, 0.5)$. In the plot, M means the total mass of the binary. The horizontal axis has no special meaning. It just indicates different NR simulations.

means the total mass of the binary system. Different numerical relativity waveforms begin at different frequency corresponding to Mf_{min} . Mf_{min} ranges from about 0.002 to 0.012. Most waveforms admit $Mf_{min} \approx 0.006$. Lower Mf_{min} means the corresponding binary system begins at larger separation and the waveform is longer. Roughly Mf_{max} falls in the quasi-normal modes stage. The specific value of Mf_{max} depends on the specific numerical simulation. In the viewpoint of the resolution requirement of the binary system in question, if the numerical resolution is higher the value of Mf_{max} is larger. Relatively the numerical setting is random, so the behavior of Mf_{max} shown in Fig. 2(b) is random.

C. Accuracy of numerical relativity waveforms with respect to LIGO

For comparison convenience, we also investigate the accuracy of numerical relativity waveforms with respect to LIGO detectors. Specifically we use the designed sensitivity of advanced LIGO [42]. The frequency band of LIGO is (10, 8192)Hz.

Note that only the numerical relativity waveform falling in the range (Mf_{min}, Mf_{max}) is trustable. Considering the source character for LIGO, we investigate $M \in (10, 200)M_{\odot}$. In Fig. 3 we show the trustable frequency range for binary system with total mass $M = 10M_{\odot}$. For other total mass systems we need only rescale the vertical axis proportional to the inverse of the system total mass $1/M$. From Fig. 3(a) we can see clearly that the numerical relativity simulation can not cover the whole frequency range of LIGO detection. This is due to the well known expensive computational cost of numerical relativity. Consequently numerical relativity only starts near merger. For early inspiral part, people rely on post-Newtonian approximation to construct the waveform template. In the current work, we just care

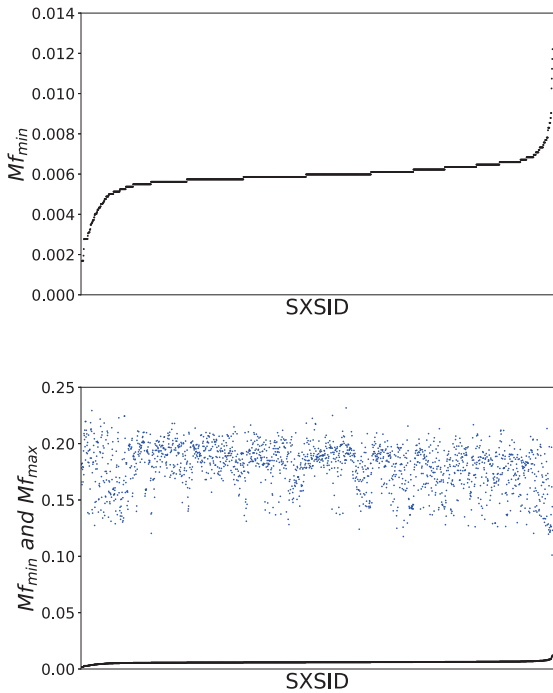


FIG. 2: Frequency lower and upper limit of the 1872 numerical relativity waveforms in SXS catalog. The top panel is the lower limit Mf_{\min} . The bottom panel shows both the lower limit (black dots) and the upper limit (blue dots).

about the accuracy of numerical relativity, so we take the integrand bound in (2) as

$$f_{\text{low}} = \max(10, f_{\min}), \quad (14)$$

$$f_{\text{up}} = \min(8192, f_{\max}). \quad (15)$$

In the first panel of Fig. 4 we plot the mismatch factors

$$\mathcal{M} \equiv 1 - \text{FF} \quad (16)$$

with respect to LIGO between the highest resolution simulation and the second highest resolution simulation.

D. Accuracy of numerical relativity waveforms with respect to space-based detectors

Regarding space-based detectors, we consider LISA [4, 43], Taiji [44] and Tianqin [45, 46] as examples. We do not involve realistic response functions as [47], instead we use sky averaged sensitivity [48] to do the estimation.

Specifically we use the following approximated sensitivity for space based gravitational wave detectors (Eq. (13) of [48])

$$S_n(f) = \frac{10}{3L^2} \left(P_{\text{OMS}} + 2(1 + \cos^2(f/f_*)) \frac{P_{\text{acc}}}{(2\pi f)^4} \right) \times$$

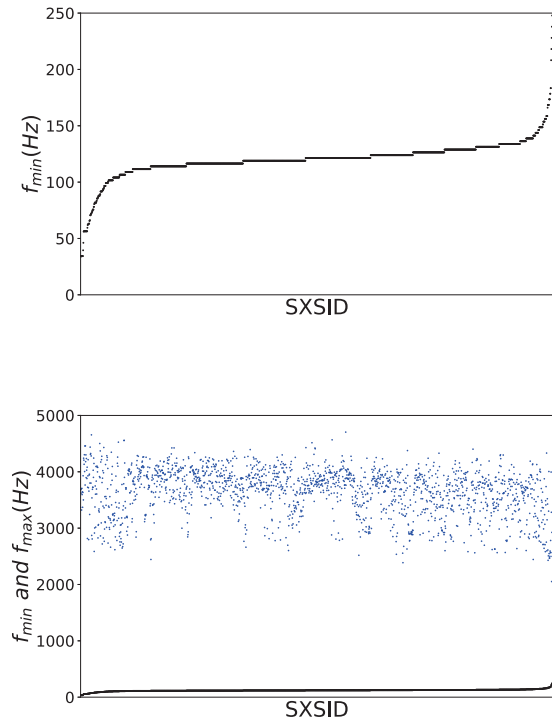


FIG. 3: Trustable frequency range of numerical relativity waveforms of the 1872 numerical relativity waveforms in SXS catalog for $M = 10M_{\odot}$ binary system. The top plot is the lower limit Mf_{\min} . The bottom plot shows both the lower limit (black dots) and the upper limit (blue dots).

$$\left(1 + \frac{6}{10} \left(\frac{f}{f_*} \right)^2 \right), \quad (17)$$

$$f_* = c/(2\pi L). \quad (18)$$

For LISA [48] we have

$$P_{\text{OMS}} = (1.5 \times 10^{-11} \text{m})^2 \text{Hz}^{-1}, \quad (19)$$

$$P_{\text{acc}} = (3 \times 10^{-15} \text{ms}^{-2})^2 \left(1 + \left(\frac{4 \times 10^{-4} \text{Hz}}{f} \right)^2 \right) \text{Hz}^{-1}, \quad (20)$$

$$L = 2.5 \times 10^9 \text{m}. \quad (21)$$

For Taiji [49] we have

$$P_{\text{OMS}} = (8 \times 10^{-12} \text{m})^2 \text{Hz}^{-1}, \quad (22)$$

$$P_{\text{acc}} = (3 \times 10^{-15} \text{ms}^{-2})^2 \left(1 + \left(\frac{4 \times 10^{-4} \text{Hz}}{f} \right)^2 \right) \text{Hz}^{-1}, \quad (23)$$

$$L = 3 \times 10^9 \text{m}. \quad (24)$$

For Tianqin we have [45]

$$P_{\text{OMS}} = (1 \times 10^{-12} \text{m})^2 \text{Hz}^{-1}, \quad (25)$$

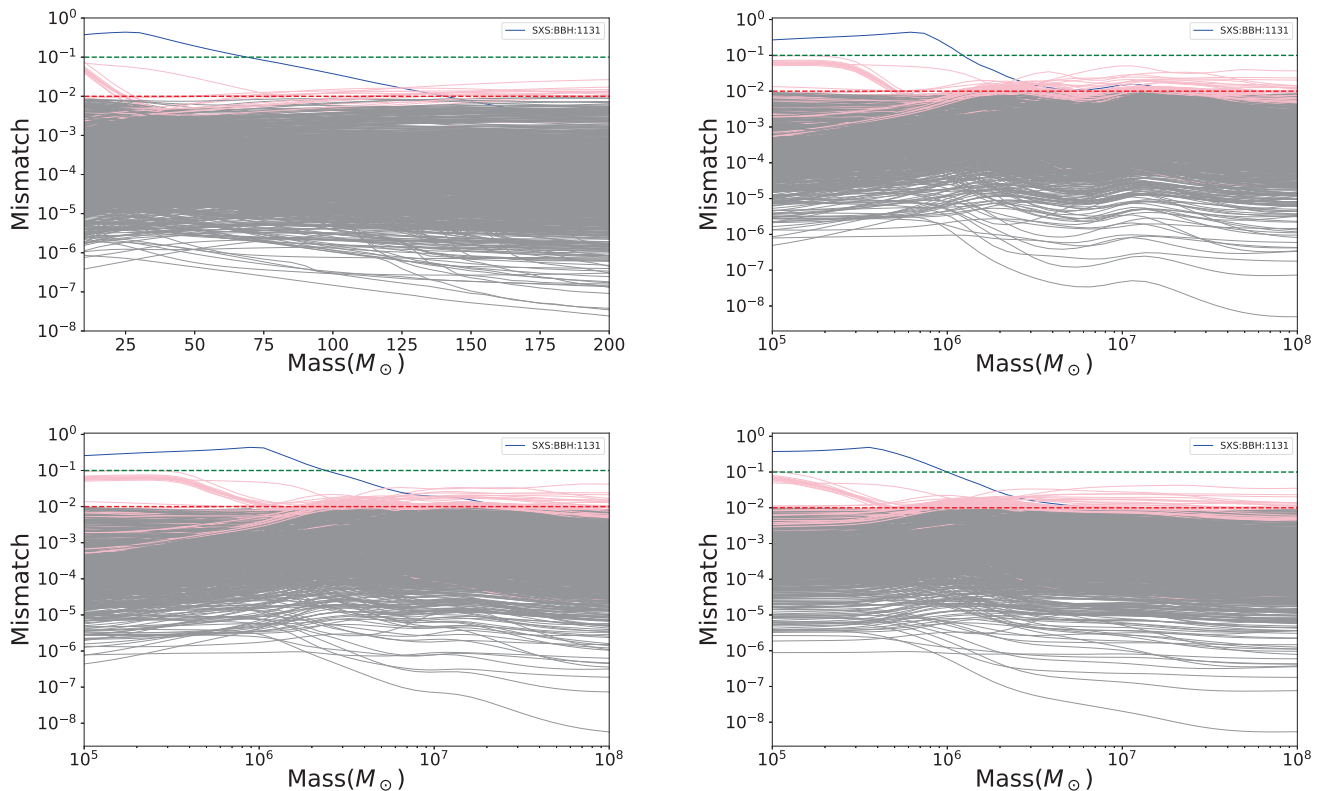


FIG. 4: The mismatch factors between the highest resolution simulation and the second highest resolution simulation. There are in all 1872 SXS waveforms are investigated here. From top to bottom, from left to right the subfigures correspond to LIGO, LISA, Taiji and Tianqin respectively. The blue lines in all of the subfigures correspond to SXS:BBH:1131.

$$P_{\text{acc}} = (1 \times 10^{-15} \text{ms}^{-2})^2 \left(1 + \left(\frac{1 \times 10^{-4} \text{Hz}}{f} \right)^2 \right) \text{Hz}^{-1}, \quad (26)$$

$$L = \sqrt{3} \times 10^8 \text{m}. \quad (27)$$

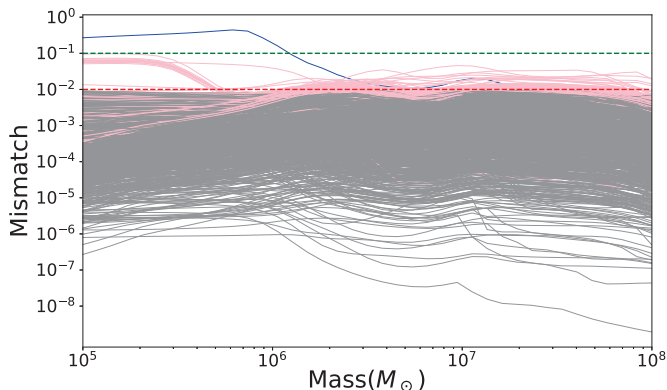


FIG. 5: Similar to Fig. 4 but with detector frequency range $(10^{-4}, 0.1) \text{Hz}$ in stead of $(10^{-5}, 1) \text{Hz}$. This plot is for LISA.

Besides the instrument noise mentioned above, there is more confusion noise due to the galaxy binaries which

can be approximated as [50]

$$S_c(f) = Af^{-7/3} e^{-f^\alpha + \beta f \sin(\kappa f)} \times [1 + \tanh(\gamma(f_k - f))] \text{Hz}^{-1} \quad (28)$$

$$A = 9 \times 10^{-45}, \quad (29)$$

$$\alpha = 0.133, \quad (30)$$

$$\beta = 243, \quad (31)$$

$$\kappa = 482, \quad (32)$$

$$\gamma = 917, \quad (33)$$

$$f_k = 0.00258. \quad (34)$$

Note that parameters $\alpha, \beta, \kappa, \gamma$ depend on observation time. The values listed above correspond to observation time half year. The overall noise sensitivity of space-based detectors can be estimated as

$$S = S_n + S_c. \quad (35)$$

Due to the similar reason for LIGO, we take the integrand bound in (2) as

$$f_{\text{low}} = \max(10^{-5}, f_{\text{min}}), \quad (36)$$

$$f_{\text{up}} = \min(1, f_{\text{max}}), \quad (37)$$

for space-based detectors.

TABLE I: Less accurate ($\mathcal{M} > 1\%$) NR simulations found in this work. Here, we list the parameters for each simulation, including mass ratio q , lowest frequency Mf_{\min} , highest frequency Mf_{\max} , and initial spin configuration. Additionally, we provide the maximum mismatch between the highest resolution simulation and the second highest resolution simulation $\max \mathcal{M}$. Here \max means the maximum value in the total mass range shown in Fig. 4. The subscriptions ‘LIGO’, ‘LISA’, ‘Taiji’ and ‘Tianqin’ are for corresponding detectors.

SXS ID	q	χ_1	χ_2	Mf_{\min}	Mf_{\max}	$\max \mathcal{M}_{\text{LIGO}}$	$\max \mathcal{M}_{\text{LISA}}$	$\max \mathcal{M}_{\text{Taiji}}$	$\max \mathcal{M}_{\text{Tianqin}}$
1415	1.50	(0.00,0.00,0.50)	(0.00,-0.00,0.50)	0.0017	0.1789	0.0756	0.0978	0.1005	0.1077
0627	1.91	(-0.51,0.44,-0.35)	(0.19,-0.01,-0.06)	0.0083	0.1626	0.0709	0.0650	0.0660	0.0491
1413	1.41	(-0.00,-0.00,0.50)	(-0.00,-0.00,0.40)	0.0017	0.1660	0.0570	0.0732	0.0755	0.0805
1414	1.83	(-0.00,-0.00,-0.50)	(0.00,-0.00,0.40)	0.0017	0.1636	0.0527	0.0695	0.0715	0.0749
1390	1.42	(0.15,0.44,-0.16)	(-0.02,0.34,0.10)	0.0017	0.1659	0.0510	0.0648	0.0672	0.0714
1393	1.79	(-0.37,-0.33,-0.00)	(-0.27,-0.39,0.11)	0.0017	0.1784	0.0490	0.0647	0.0667	0.0694
1392	1.51	(-0.40,0.23,0.17)	(0.35,-0.13,-0.25)	0.0017	0.1795	0.0478	0.0625	0.0642	0.0679
1389	1.63	(-0.29,0.20,-0.30)	(-0.01,0.42,0.16)	0.0017	0.1771	0.0460	0.0594	0.0613	0.0651
1391	1.83	(-0.15,0.29,-0.33)	(-0.33,-0.29,-0.03)	0.0017	0.1813	0.0440	0.0566	0.0583	0.0619
1412	1.63	(-0.00,-0.00,0.40)	(-0.00,0.00,-0.30)	0.0017	0.1822	0.0421	0.0562	0.0578	0.0606
1416	1.78	(0.00,-0.00,-0.40)	(-0.00,0.00,-0.40)	0.0017	0.1825	0.0392	0.0524	0.0539	0.0561
1926	4.00	(0.76,0.26,0.04)	(0.00,-0.14,0.79)	0.0065	0.1943	0.0266	0.0350	0.0337	0.0335
2000	4.00	(-0.40,0.69,0.08)	(0.45,0.65,-0.11)	0.0066	0.1902	0.0171	0.0206	0.0204	0.0204
1992	4.00	(-0.61,0.07,-0.51)	(-0.27,0.75,-0.05)	0.0062	0.1733	0.0162	0.0192	0.0195	0.0194
2044	4.00	(0.74,-0.29,0.11)	(0.14,-0.60,0.52)	0.0067	0.1890	0.0148	0.0151	0.0149	0.0140
1991	4.00	(-0.26,-0.51,-0.56)	(-0.07,0.06,0.79)	0.0061	0.1724	0.0136	0.0201	0.0219	0.0221
2038	4.00	(-0.80,-0.05,0.05)	(-0.01,-0.08,-0.39)	0.0065	0.1920	0.0135	0.0249	0.0244	0.0246
2054	4.00	(0.66,-0.45,0.08)	(0.38,-0.31,0.63)	0.0065	0.1887	0.0135	0.0199	0.0190	0.0192
2074	4.00	(-0.66,0.44,0.07)	(-0.74,0.28,0.10)	0.0066	0.1548	0.0127	0.0214	0.0210	0.0211
1987	4.00	(0.38,0.43,-0.55)	(0.54,0.58,0.04)	0.0062	0.1659	0.0119	0.0160	0.0177	0.0182
1110	7.00	(-0.00,-0.00,0.00)	(-0.00,-0.00,-0.00)	0.0023	0.1724	0.0106	0.0510	0.0423	0.0427
1928	4.00	(-0.33,0.72,0.07)	(0.62,0.48,-0.13)	0.0065	0.1898	0.0104	0.0114	0.0115	0.0113
1978	4.00	(0.50,0.26,0.57)	(-0.77,-0.20,0.03)	0.0070	0.1438	0.0092	0.0171	0.0168	0.0179
1135	1.00	(-0.00,-0.00,-0.44)	(-0.00,0.00,-0.44)	0.0073	0.1355	0.0089	0.0134	0.0137	0.0097
1623	3.93	(0.02,0.55,0.43)	(-0.56,-0.33,-0.45)	0.0066	0.1863	0.0089	0.0187	0.0184	0.0176
1993	4.00	(-0.06,-0.58,-0.54)	(-0.24,-0.76,0.02)	0.0062	0.1439	0.0087	0.0109	0.0116	0.0121
1994	4.00	(0.58,0.16,-0.53)	(0.11,-0.79,-0.08)	0.0062	0.1938	0.0085	0.0121	0.0118	0.0108
1981	4.00	(0.26,-0.55,-0.52)	(-0.35,-0.72,-0.02)	0.0062	0.1460	0.0081	0.0120	0.0114	0.0101
1156	4.39	(-0.16,0.21,0.38)	(0.53,-0.55,0.11)	0.0041	0.1776	0.0079	0.0085	0.0088	0.0106
1629	3.46	(0.54,0.15,-0.45)	(-0.23,0.08,-0.73)	0.0059	0.2096	0.0077	0.0089	0.0097	0.0104
1923	4.00	(-0.79,0.04,0.09)	(-0.75,0.28,0.02)	0.0066	0.1622	0.0074	0.0188	0.0184	0.0169
2011	4.00	(0.79,-0.09,0.03)	(0.37,0.69,0.18)	0.0063	0.2168	0.0064	0.0292	0.0260	0.0243
1863	3.63	(-0.45,0.30,-0.58)	(0.33,0.33,0.43)	0.0060	0.1654	0.0063	0.0114	0.0133	0.0137
1997	4.00	(-0.76,-0.24,0.04)	(-0.00,0.14,0.79)	0.0063	0.1663	0.0060	0.0114	0.0104	0.0101
1983	4.00	(-0.47,0.35,-0.55)	(-0.52,-0.59,0.14)	0.0062	0.1721	0.0058	0.0130	0.0136	0.0144
2005	4.00	(0.36,0.71,0.07)	(0.48,0.64,0.06)	0.0065	0.1290	0.0057	0.0136	0.0130	0.0119
2081	4.00	(-0.36,0.71,0.06)	(0.62,0.49,-0.14)	0.0065	0.1904	0.0055	0.0104	0.0105	0.0112
2048	4.00	(0.80,-0.02,0.02)	(-0.26,0.41,0.64)	0.0065	0.1924	0.0054	0.0092	0.0100	0.0102
1579	3.44	(0.21,0.46,-0.38)	(0.18,0.48,-0.59)	0.0062	0.1837	0.0053	0.0137	0.0145	0.0153
1986	4.00	(-0.39,0.45,-0.53)	(0.11,0.03,0.79)	0.0063	0.1412	0.0052	0.0123	0.0120	0.0108
2007	4.00	(0.77,0.22,0.04)	(0.00,0.15,-0.79)	0.0063	0.1887	0.0051	0.0123	0.0124	0.0136
1979	4.00	(-0.53,0.00,0.60)	(-0.03,-0.12,-0.79)	0.0067	0.1697	0.0050	0.0133	0.0132	0.0137
2043	4.00	(-0.70,-0.39,0.06)	(-0.50,0.34,0.52)	0.0063	0.1638	0.0050	0.0107	0.0104	0.0105
1975	4.00	(0.45,0.27,0.61)	(0.04,-0.13,0.79)	0.0071	0.1899	0.0049	0.0181	0.0190	0.0200
1917	4.00	(0.38,0.71,0.01)	(-0.68,0.36,0.20)	0.0066	0.1862	0.0046	0.0101	0.0105	0.0113
1972	4.00	(-0.50,0.20,0.59)	(0.80,0.00,-0.06)	0.0068	0.2032	0.0044	0.0094	0.0099	0.0103
1974	4.00	(-0.34,0.43,0.59)	(-0.00,-0.00,-0.00)	0.0068	0.2039	0.0044	0.0162	0.0177	0.0190
0147	1.00	(0.40,0.29,-0.00)	(-0.40,-0.29,-0.00)	0.0107	0.1616	0.0043	0.0104	0.0099	0.0093
2015	4.00	(0.57,0.56,0.03)	(0.04,-0.07,0.39)	0.0065	0.1731	0.0042	0.0110	0.0107	0.0101
0469	1.00	(-0.16,0.78,0.03)	(0.04,-0.01,0.40)	0.0059	0.1842	0.0039	0.0111	0.0120	0.0132
1927	4.00	(0.52,-0.61,0.01)	(0.03,0.79,0.10)	0.0063	0.1738	0.0037	0.0213	0.0189	0.0169
2034	4.00	(-0.79,-0.07,0.06)	(0.39,0.07,-0.03)	0.0066	0.1860	0.0036	0.0121	0.0124	0.0133
2010	4.00	(0.78,0.16,0.02)	(0.23,0.75,0.16)	0.0065	0.1819	0.0033	0.0112	0.0101	0.0114

to next page

TABLE I continue

SXS ID	q	χ_1	χ_2	Mf_{\min}	Mf_{\max}	$\max \mathcal{M}_{\text{LIGO}}$	$\max \mathcal{M}_{\text{LISA}}$	$\max \mathcal{M}_{\text{Taiji}}$	$\max \mathcal{M}_{\text{Tianqin}}$
1973	4.00	(0.29,0.47,0.58)	(-0.08,0.07,-0.79)	0.0067	0.1823	0.0029	0.0132	0.0138	0.0150
1614	2.68	(0.20,0.03,0.71)	(-0.11,-0.07,0.03)	0.0063	0.1896	0.0028	0.0118	0.0121	0.0134
1713	3.97	(0.05,-0.47,0.30)	(0.68,-0.16,-0.34)	0.0066	0.1842	0.0028	0.0092	0.0092	0.0100
1741	2.77	(0.58,-0.51,-0.06)	(-0.01,-0.05,-0.45)	0.0061	0.1964	0.0027	0.0092	0.0098	0.0105
2079	4.00	(-0.39,-0.69,0.04)	(-0.31,0.73,-0.12)	0.0066	0.1948	0.0027	0.0158	0.0131	0.0132
1209	2.00	(0.06,-0.01,0.85)	(-0.19,0.83,0.01)	0.0062	0.1864	0.0026	0.0093	0.0097	0.0107
2004	4.00	(-0.27,-0.75,0.02)	(-0.22,0.77,-0.09)	0.0063	0.2052	0.0026	0.0111	0.0107	0.0094
2064	4.00	(-0.44,-0.67,0.00)	(0.24,-0.61,-0.46)	0.0063	0.1698	0.0023	0.0102	0.0094	0.0089
0705	2.00	(-0.03,-0.04,0.80)	(0.76,-0.26,0.02)	0.0062	0.1925	0.0022	0.0105	0.0113	0.0125
1095	2.00	(0.22,0.77,0.02)	(-0.09,0.04,-0.79)	0.0057	0.1743	0.0022	0.0124	0.0119	0.0100
1659	3.47	(-0.07,0.58,0.54)	(-0.04,0.17,0.43)	0.0066	0.1842	0.0022	0.0111	0.0110	0.0113
2058	4.00	(-0.18,0.78,0.03)	(0.35,-0.33,-0.64)	0.0062	0.1803	0.0022	0.0103	0.0097	0.0086
1591	3.59	(0.31,-0.28,0.50)	(0.48,-0.11,0.32)	0.0066	0.1906	0.0020	0.0123	0.0121	0.0130
1399	1.58	(-0.29,-0.20,-0.23)	(-0.37,0.03,0.20)	0.0028	0.2196	0.0019	0.0108	0.0118	0.0125
0708	2.00	(0.76,-0.23,0.04)	(-0.06,-0.10,0.79)	0.0061	0.1620	0.0018	0.0108	0.0105	0.0094
0968	2.00	(0.07,0.80,-0.01)	(-0.60,0.51,0.10)	0.0059	0.1737	0.0018	0.0088	0.0093	0.0102
0888	2.00	(-0.61,-0.51,0.03)	(-0.20,-0.42,0.65)	0.0061	0.1805	0.0017	0.0127	0.0123	0.0102
1839	3.76	(0.25,-0.33,0.50)	(0.18,-0.54,-0.37)	0.0066	0.1715	0.0017	0.0106	0.0104	0.0112
0835	2.00	(-0.48,-0.64,0.02)	(0.00,-0.00,0.00)	0.0059	0.1907	0.0016	0.0097	0.0108	0.0118
0900	2.00	(-0.15,0.79,0.04)	(-0.30,0.38,0.64)	0.0061	0.1952	0.0016	0.0086	0.0096	0.0103
1532	3.02	(-0.59,-0.29,0.39)	(0.17,0.12,-0.31)	0.0065	0.1981	0.0015	0.0116	0.0114	0.0106
1668	3.43	(0.38,0.13,-0.66)	(-0.43,-0.63,0.07)	0.0061	0.1434	0.0015	0.0103	0.0094	0.0082
1929	4.00	(0.43,-0.67,0.08)	(0.65,-0.45,0.15)	0.0067	0.1835	0.0014	0.0122	0.0114	0.0097
0733	2.00	(0.35,-0.19,-0.02)	(-0.11,0.79,0.06)	0.0060	0.2009	0.0012	0.0108	0.0105	0.0093
1656	3.40	(-0.37,0.19,0.59)	(-0.06,-0.08,-0.12)	0.0066	0.1810	0.0012	0.0118	0.0124	0.0134
0664	1.33	(-0.79,-0.12,0.03)	(-0.79,-0.10,0.03)	0.0056	0.1881	0.0011	0.0094	0.0100	0.0109
1006	1.03	(0.64,0.21,-0.35)	(-0.48,0.18,0.50)	0.0059	0.1814	0.0011	0.0112	0.0109	0.0099
1557	2.94	(0.69,-0.07,0.20)	(-0.04,0.79,-0.13)	0.0062	0.1887	0.0011	0.0137	0.0135	0.0136
1696	2.63	(0.67,0.33,0.09)	(-0.12,0.16,0.27)	0.0062	0.1709	0.0011	0.0113	0.0108	0.0091
1770	2.55	(0.42,0.28,0.58)	(-0.33,0.63,-0.34)	0.0063	0.1912	0.0011	0.0112	0.0116	0.0127
1787	3.23	(0.59,0.37,0.27)	(0.14,0.30,-0.67)	0.0063	0.1954	0.0011	0.0122	0.0119	0.0108
0834	1.00	(-0.56,-0.57,0.03)	(-0.00,0.00,-0.00)	0.0057	0.2074	0.0010	0.0099	0.0103	0.0114
0907	1.00	(-0.73,-0.33,-0.02)	(0.53,-0.05,0.60)	0.0059	0.2097	0.0010	0.0117	0.0125	0.0135
1206	1.00	(0.62,-0.58,-0.05)	(0.18,0.83,0.08)	0.0057	0.1797	0.0010	0.0099	0.0102	0.0112
0905	1.00	(0.65,-0.46,0.02)	(0.49,-0.11,0.62)	0.0059	0.1925	0.0009	0.0110	0.0108	0.0116
0916	1.00	(-0.77,-0.21,0.01)	(-0.56,-0.57,0.08)	0.0057	0.1979	0.0009	0.0097	0.0101	0.0110
0966	2.00	(-0.71,-0.37,0.06)	(-0.68,0.42,-0.06)	0.0060	0.2054	0.0009	0.0109	0.0115	0.0125
1149	3.00	(0.00,-0.00,0.70)	(-0.00,-0.00,0.60)	0.0063	0.1798	0.0009	0.0132	0.0130	0.0142
1523	2.93	(0.49,-0.26,0.46)	(0.41,0.30,0.40)	0.0065	0.1963	0.0009	0.0100	0.0107	0.0117
0750	2.00	(-0.28,-0.48,0.57)	(0.07,-0.05,-0.80)	0.0060	0.1768	0.0008	0.0109	0.0111	0.0118
1000	1.21	(0.31,0.63,0.34)	(-0.60,-0.02,0.48)	0.0060	0.1853	0.0008	0.0105	0.0103	0.0093
1086	1.07	(-0.33,-0.35,0.63)	(0.59,0.18,0.16)	0.0060	0.1990	0.0008	0.0112	0.0115	0.0126
1197	2.00	(-0.78,-0.34,-0.04)	(0.65,-0.54,0.10)	0.0059	0.1903	0.0008	0.0098	0.0102	0.0111
1199	2.00	(0.68,-0.51,0.04)	(0.10,0.08,-0.84)	0.0057	0.2148	0.0008	0.0093	0.0092	0.0101
1849	2.70	(0.54,-0.00,0.53)	(-0.41,0.31,0.34)	0.0063	0.1963	0.0008	0.0106	0.0103	0.0094
2131	2.00	(0.00,0.00,0.85)	(0.00,-0.00,0.85)	0.0060	0.1824	0.0008	0.0133	0.0142	0.0156
0601	1.06	(-0.50,0.07,0.59)	(0.02,0.04,0.66)	0.0061	0.1974	0.0007	0.0091	0.0095	0.0105
0635	1.00	(0.67,-0.44,0.03)	(-0.06,-0.04,0.80)	0.0059	0.1930	0.0007	0.0106	0.0111	0.0119
0170	1.00	(-0.00,-0.00,0.44)	(0.00,0.00,0.44)	0.0071	0.1582	0.0006	0.0110	0.0109	0.0121
0323	1.22	(0.00,-0.00,0.33)	(-0.00,-0.00,-0.44)	0.0066	0.1553	0.0006	0.0097	0.0095	0.0105
0781	2.00	(0.79,-0.14,0.03)	(0.05,0.10,-0.79)	0.0057	0.2059	0.0006	0.0118	0.0116	0.0108
1071	1.07	(-0.13,0.20,0.66)	(0.33,-0.56,0.39)	0.0060	0.1995	0.0006	0.0124	0.0133	0.0145
1716	2.24	(-0.29,0.36,0.53)	(-0.55,-0.08,0.46)	0.0062	0.1936	0.0006	0.0095	0.0102	0.0112
0256	2.00	(-0.00,0.00,0.60)	(-0.00,0.00,0.60)	0.0057	0.1609	0.0005	0.0116	0.0121	0.0133
0351	1.00	(-0.20,0.77,0.03)	(0.08,-0.01,0.80)	0.0060	0.1906	0.0005	0.0115	0.0113	0.0108
0936	2.00	(-0.68,-0.42,-0.01)	(0.79,0.08,0.04)	0.0060	0.1985	0.0005	0.0104	0.0110	0.0120
0948	2.00	(0.03,0.01,0.80)	(-0.42,0.38,-0.56)	0.0061	0.1913	0.0005	0.0095	0.0094	0.0101
1014	1.69	(-0.64,0.10,0.33)	(-0.54,0.09,0.46)	0.0061	0.2025	0.0005	0.0123	0.0121	0.0128
1632	3.01	(0.55,-0.51,0.25)	(-0.63,-0.13,-0.33)	0.0062	0.1970	0.0005	0.0133	0.0136	0.0147
1718	2.31	(-0.30,0.33,0.61)	(-0.38,0.64,-0.09)	0.0062	0.1832	0.0005	0.0108	0.0106	0.0105

to next page

TABLE I continue

SXS ID	q	χ_1	χ_2	Mf_{\min}	Mf_{\max}	$\max \mathcal{M}_{\text{LIGO}}$	$\max \mathcal{M}_{\text{LISA}}$	$\max \mathcal{M}_{\text{Taiji}}$	$\max \mathcal{M}_{\text{Tianqin}}$
2006	4.00	(-0.49,-0.63,-0.02)	(0.75,-0.23,0.14)	0.0063	0.1810	0.0005	0.0111	0.0093	0.0085
0065	8.00	(-0.00,-0.00,0.50)	(0.00,0.00,0.00)	0.0067	0.1400	0.0004	0.0115	0.0111	0.0094
0324	1.22	(-0.00,-0.00,0.33)	(-0.00,-0.00,-0.44)	0.0088	0.1277	0.0004	0.0101	0.0098	0.0098
0374	2.00	(-0.26,0.47,0.59)	(0.00,-0.00,0.00)	0.0062	0.1868	0.0004	0.0099	0.0103	0.0113
0383	1.75	(-0.31,0.74,0.04)	(0.10,0.01,0.79)	0.0060	0.1942	0.0004	0.0108	0.0107	0.0113
0476	1.00	(-0.17,0.37,0.44)	(0.04,0.00,0.80)	0.0061	0.1891	0.0004	0.0142	0.0148	0.0162
0662	1.33	(-0.68,-0.41,0.03)	(-0.02,0.09,0.79)	0.0060	0.1899	0.0004	0.0099	0.0103	0.0112
0688	1.67	(-0.65,-0.46,0.03)	(-0.03,0.10,0.79)	0.0061	0.1686	0.0004	0.0101	0.0098	0.0090
0772	2.00	(-0.45,0.66,0.08)	(-0.14,0.79,0.01)	0.0060	0.1960	0.0004	0.0130	0.0137	0.0148
0845	2.00	(0.74,-0.30,0.04)	(-0.04,-0.05,0.40)	0.0061	0.2014	0.0004	0.0130	0.0138	0.0148
0941	2.00	(-0.03,0.03,0.80)	(-0.05,-0.57,-0.56)	0.0062	0.1785	0.0004	0.0094	0.0100	0.0111
0988	2.00	(-0.04,0.03,0.80)	(-0.20,-0.77,0.02)	0.0062	0.1619	0.0004	0.0090	0.0096	0.0106
1090	1.59	(-0.30,-0.33,0.48)	(-0.30,-0.34,0.52)	0.0061	0.1891	0.0004	0.0117	0.0126	0.0139
1529	3.14	(0.33,-0.59,0.13)	(-0.38,0.50,0.48)	0.0063	0.1636	0.0004	0.0102	0.0095	0.0079
1642	3.29	(-0.30,-0.54,0.26)	(0.72,-0.15,0.04)	0.0066	0.1904	0.0004	0.0137	0.0132	0.0112
1676	3.25	(0.11,0.18,0.44)	(0.31,-0.13,0.22)	0.0066	0.2032	0.0004	0.0108	0.0106	0.0107
1692	2.88	(-0.51,0.31,-0.02)	(-0.34,-0.41,-0.07)	0.0060	0.1886	0.0004	0.0111	0.0108	0.0094
0333	2.00	(0.00,0.00,0.80)	(-0.00,0.00,0.80)	0.0063	0.1786	0.0003	0.0120	0.0129	0.0143
0348	1.19	(-0.21,0.45,0.60)	(0.06,0.01,0.76)	0.0061	0.1781	0.0003	0.0116	0.0114	0.0120
0478	1.32	(-0.23,0.63,0.14)	(0.08,-0.00,0.78)	0.0060	0.1859	0.0003	0.0134	0.0131	0.0118
0571	1.09	(0.00,0.08,-0.02)	(-0.00,0.00,-0.29)	0.0057	0.1986	0.0003	0.0091	0.0094	0.0104
0575	1.20	(-0.00,0.01,0.39)	(0.00,-0.00,0.14)	0.0059	0.1901	0.0003	0.0105	0.0111	0.0123
0691	1.67	(-0.73,-0.31,0.06)	(0.02,0.80,-0.07)	0.0059	0.1792	0.0003	0.0104	0.0101	0.0088
0745	2.00	(-0.16,-0.52,0.59)	(-0.00,0.00,0.00)	0.0062	0.2040	0.0003	0.0087	0.0094	0.0103
0830	2.00	(0.70,-0.38,0.06)	(-0.65,-0.46,-0.08)	0.0059	0.1802	0.0003	0.0123	0.0118	0.0099
0859	1.00	(-0.01,0.04,0.80)	(-0.34,-0.21,0.01)	0.0060	0.1943	0.0003	0.0128	0.0126	0.0128
0991	2.00	(-0.67,-0.44,0.03)	(-0.32,-0.72,0.12)	0.0060	0.2002	0.0003	0.0121	0.0131	0.0142
1011	1.53	(0.51,0.31,0.31)	(0.33,0.48,0.48)	0.0060	0.1857	0.0003	0.0126	0.0132	0.0145
1020	1.24	(0.37,0.38,0.49)	(0.53,-0.27,0.52)	0.0060	0.1910	0.0003	0.0095	0.0100	0.0108
1023	1.22	(-0.59,-0.02,0.36)	(0.21,-0.63,-0.37)	0.0057	0.1880	0.0003	0.0089	0.0093	0.0102
1063	1.78	(-0.47,0.28,-0.29)	(-0.29,-0.41,0.58)	0.0059	0.1965	0.0003	0.0097	0.0103	0.0113
1070	1.20	(-0.15,-0.43,0.64)	(-0.42,-0.41,-0.49)	0.0059	0.1691	0.0003	0.0107	0.0111	0.0122
1571	3.44	(-0.28,-0.35,0.64)	(0.48,-0.51,-0.10)	0.0068	0.1777	0.0003	0.0087	0.0093	0.0102
1616	2.87	(0.53,0.30,0.42)	(-0.38,0.02,-0.54)	0.0062	0.2089	0.0003	0.0128	0.0137	0.0149
1709	3.44	(-0.09,0.20,0.29)	(0.14,0.47,-0.60)	0.0065	0.1871	0.0003	0.0101	0.0098	0.0097
1930	4.00	(0.09,0.79,0.04)	(-0.17,0.07,-0.78)	0.0065	0.2064	0.0003	0.0103	0.0089	0.0081
2161	3.00	(0.00,-0.00,0.60)	(0.00,0.00,0.00)	0.0057	0.1913	0.0003	0.0118	0.0116	0.0125
0178	1.00	(0.00,0.00,0.99)	(-0.00,-0.00,0.99)	0.0056	0.1941	0.0002	0.0144	0.0151	0.0165
0372	1.50	(0.00,-0.00,0.80)	(-0.00,0.00,-0.40)	0.0060	0.1851	0.0002	0.0088	0.0093	0.0102
0395	1.00	(-0.10,0.42,-0.42)	(0.04,-0.01,0.80)	0.0059	0.2164	0.0002	0.0095	0.0101	0.0110
0408	2.00	(-0.29,0.53,0.02)	(0.08,0.01,0.80)	0.0061	0.1909	0.0002	0.0113	0.0123	0.0135
0505	1.85	(-0.26,0.51,0.09)	(0.08,0.01,0.79)	0.0061	0.2000	0.0002	0.0090	0.0095	0.0104
0655	1.33	(0.61,-0.52,0.03)	(0.00,0.00,-0.00)	0.0057	0.2062	0.0002	0.0113	0.0119	0.0130
0679	1.67	(-0.04,-0.04,0.80)	(0.79,-0.14,0.03)	0.0062	0.1587	0.0002	0.0118	0.0124	0.0137
0774	2.00	(0.79,-0.12,0.02)	(-0.00,-0.00,0.00)	0.0059	0.1851	0.0002	0.0107	0.0104	0.0089
0777	2.00	(0.80,0.05,0.07)	(0.75,-0.29,0.01)	0.0059	0.2001	0.0002	0.0127	0.0125	0.0120
0870	1.00	(0.04,-0.01,0.80)	(-0.02,0.40,0.01)	0.0060	0.1930	0.0002	0.0103	0.0106	0.0117
0957	2.00	(-0.73,-0.33,0.00)	(0.58,-0.07,-0.54)	0.0059	0.1765	0.0002	0.0110	0.0105	0.0090
0963	1.00	(0.58,-0.55,-0.00)	(-0.57,0.56,0.00)	0.0057	0.2067	0.0002	0.0108	0.0105	0.0097
1084	1.76	(0.48,-0.16,0.48)	(-0.73,0.10,0.30)	0.0061	0.1841	0.0002	0.0131	0.0128	0.0116
1196	1.00	(0.64,-0.55,0.06)	(0.64,-0.55,0.06)	0.0057	0.1681	0.0002	0.0110	0.0115	0.0126
1406	1.60	(-0.29,0.29,0.24)	(-0.38,-0.01,0.15)	0.0028	0.1984	0.0002	0.0103	0.0110	0.0120
1495	1.00	(-0.00,-0.00,0.78)	(0.00,0.00,0.53)	0.0061	0.1920	0.0002	0.0124	0.0132	0.0144
1518	2.08	(0.23,-0.66,0.08)	(-0.60,-0.17,0.15)	0.0059	0.1989	0.0002	0.0109	0.0113	0.0123
1645	2.29	(-0.33,-0.38,0.45)	(0.00,-0.64,0.46)	0.0062	0.1917	0.0002	0.0115	0.0113	0.0113
1852	3.03	(-0.45,0.25,0.46)	(-0.15,0.71,-0.25)	0.0063	0.1921	0.0002	0.0096	0.0099	0.0108
1860	3.42	(-0.35,-0.20,0.64)	(0.67,0.33,-0.24)	0.0067	0.1779	0.0002	0.0106	0.0112	0.0123
2097	1.00	(-0.00,0.00,0.30)	(0.00,-0.00,-0.00)	0.0051	0.2019	0.0002	0.0098	0.0105	0.0116
2125	2.00	(0.00,-0.00,0.30)	(0.00,-0.00,0.30)	0.0056	0.2023	0.0002	0.0105	0.0104	0.0115
0155	1.00	(-0.00,-0.00,0.80)	(0.00,0.00,0.80)	0.0055	0.1886	0.0001	0.0123	0.0130	0.0143

to next page

TABLE I continue

SXS ID	q	χ_1	χ_2	Mf_{\min}	Mf_{\max}	$\max \mathcal{M}_{\text{LIGO}}$	$\max \mathcal{M}_{\text{LISA}}$	$\max \mathcal{M}_{\text{Taiji}}$	$\max \mathcal{M}_{\text{Tianqin}}$
0179	1.50	(-0.00,-0.00,0.99)	(0.13,0.05,0.14)	0.0056	0.1677	0.0001	0.0126	0.0130	0.0144
0328	1.00	(0.00,0.00,0.80)	(-0.00,-0.00,0.80)	0.0062	0.1871	0.0001	0.0100	0.0105	0.0115
0415	1.00	(0.00,0.00,-0.00)	(-0.00,0.00,-0.40)	0.0056	0.1978	0.0001	0.0089	0.0092	0.0102
0495	1.38	(-0.03,0.13,0.01)	(0.01,-0.00,0.40)	0.0059	0.1862	0.0001	0.0094	0.0100	0.0111
0564	1.69	(-0.01,0.01,0.27)	(0.00,0.00,0.61)	0.0061	0.1912	0.0001	0.0089	0.0091	0.0101
0681	1.67	(0.06,-0.01,0.80)	(-0.28,0.75,0.03)	0.0062	0.1897	0.0001	0.0122	0.0129	0.0142
0694	1.67	(-0.07,0.80,0.03)	(0.10,-0.02,0.79)	0.0060	0.1938	0.0001	0.0119	0.0118	0.0124
0706	2.00	(-0.02,0.05,0.80)	(-0.40,-0.69,0.03)	0.0063	0.1693	0.0001	0.0111	0.0116	0.0128
0752	2.00	(-0.39,0.42,0.56)	(-0.48,-0.63,0.12)	0.0062	0.1830	0.0001	0.0107	0.0105	0.0109
0854	2.00	(0.70,-0.39,0.04)	(0.36,-0.18,0.02)	0.0059	0.1927	0.0001	0.0138	0.0135	0.0121
0915	2.00	(0.71,-0.36,0.08)	(-0.30,-0.74,-0.07)	0.0059	0.1865	0.0001	0.0108	0.0104	0.0091
0964	2.00	(0.70,-0.38,0.01)	(-0.73,0.33,-0.01)	0.0060	0.1770	0.0001	0.0116	0.0112	0.0093
1044	1.77	(0.66,0.08,-0.25)	(-0.03,-0.74,0.26)	0.0057	0.2069	0.0001	0.0090	0.0095	0.0104
1068	1.46	(0.08,0.02,0.19)	(-0.63,0.02,0.43)	0.0060	0.1909	0.0001	0.0095	0.0100	0.0111
1194	2.00	(0.75,-0.39,0.07)	(-0.68,-0.49,-0.09)	0.0059	0.1840	0.0001	0.0104	0.0100	0.0083
1477	1.00	(-0.00,-0.00,0.80)	(0.00,0.00,0.80)	0.0062	0.1879	0.0001	0.0094	0.0100	0.0110
1521	3.07	(-0.38,0.26,0.39)	(0.36,0.44,0.28)	0.0065	0.1469	0.0001	0.0097	0.0103	0.0114
1747	2.66	(-0.21,-0.00,0.70)	(-0.09,0.16,-0.39)	0.0065	0.1829	0.0001	0.0119	0.0122	0.0135
1893	2.62	(0.30,0.51,0.51)	(-0.31,-0.17,0.71)	0.0065	0.1882	0.0001	0.0136	0.0134	0.0128
2156	3.00	(-0.00,0.00,0.40)	(-0.00,0.00,-0.60)	0.0059	0.1788	0.0001	0.0103	0.0101	0.0106
0255	2.00	(0.00,-0.00,0.60)	(0.00,-0.00,-0.00)	0.0056	0.1788	0.0000	0.0110	0.0114	0.0125
0418	1.00	(0.00,0.00,-0.00)	(-0.00,-0.00,0.40)	0.0059	0.1858	0.0000	0.0090	0.0094	0.0105
0553	1.07	(-0.01,0.03,0.69)	(0.00,0.00,0.46)	0.0061	0.1864	0.0000	0.0091	0.0096	0.0106
0581	1.68	(-0.21,0.55,0.50)	(0.01,0.00,0.07)	0.0061	0.1932	0.0000	0.0117	0.0119	0.0132
0607	1.50	(-0.04,0.20,0.22)	(-0.12,0.37,0.22)	0.0060	0.1865	0.0000	0.0098	0.0103	0.0112
2101	1.00	(-0.00,0.00,0.60)	(0.00,-0.00,0.00)	0.0052	0.2245	0.0000	0.0104	0.0111	0.0123

NR waveforms have a critical limitation that they are some short (due to the computational cost) and mainly focus on the merger phase. Especially for the gravitational waves emitted by supermassive black hole binaries, the majority of the evolution occurs in the inspiral phase. Therefore, simply calculating the accuracy of NR waveforms will lose the important inspiral phase, which will affect the results of the accuracy of the waveforms. In future work, we plan to use the PN(Post-Newtonian)-NR waveform models including SEOBNR, SEOBNRE and others to investigate the waveform template accuracy for space-based detectors.

The corresponding mismatch factors between the highest resolution simulation and the second highest resolution simulation for LISA, Taiji and Tianqin are shown in Fig. 4. Similar to the situation for LIGO, most NR simulations admit accuracy better than 99%. A few NR simulations have less accuracy. We list these less accurate simulations in Tab. I.

From Fig. 4, we can see SXS:BBH:1131 has very large mismatch factor. This means ones must take caution when using SXS:BBH:1131 result. For other simulations listed in Tab. I, ones also have to note the specific accuracy requirement when using those simulation results.

For all lines of Fig. 4, there is a typical behavior that the line increases along with the black hole mass and then decreases. We can understand this fact as follows. Due to the numerical error accumulation, the merger part of the waveform corresponds to the least accurate part of the waveform. Due to the resolution requirement of the sim-

ulation, the merger part is also the least accurate part of the waveform. In the frequency domain, when the black hole mass increases, the merger part moves from right to left. Note that the most sensitive range of the detector locates at the center. For relative small mass BBHs, the merger part waveform locates at the right side of the aforementioned sensitive frequency range. When black hole mass increases, the merger part falls into the sensitive frequency range. Consequently the mismatch factor increases. When the black hole mass increases more, the merger part waveform leaves the sensitive frequency range. So the mismatch factor decreases consequently.

Comparing to the result for LIGO, we find that the numerical relativity accuracy for space-based detectors is comparable to that for ground-based detectors. That is to say if the accuracy requirement is similar to that of LIGO, the current numerical relativity simulation results can satisfy the need of space-based detectors.

Considering that the frequency range of space-based detector may not reach $(10^{-5}, 1)\text{Hz}$, we have also calculated the mismatch factor with replacing (36) and (37) with

$$f_{\text{low}} = \max(10^{-4}, f_{\min}), \quad (38)$$

$$f_{\text{up}} = \min(0.1, f_{\max}). \quad (39)$$

The results are almost the same as Fig. 4. Since the results for LISA, Taiji and Tianqin are similar to each other, we only plot LISA as the example in Fig. 5.

The frequency range of numerical relativity waveform shown in Fig. 1 is the most optimal one. We can see

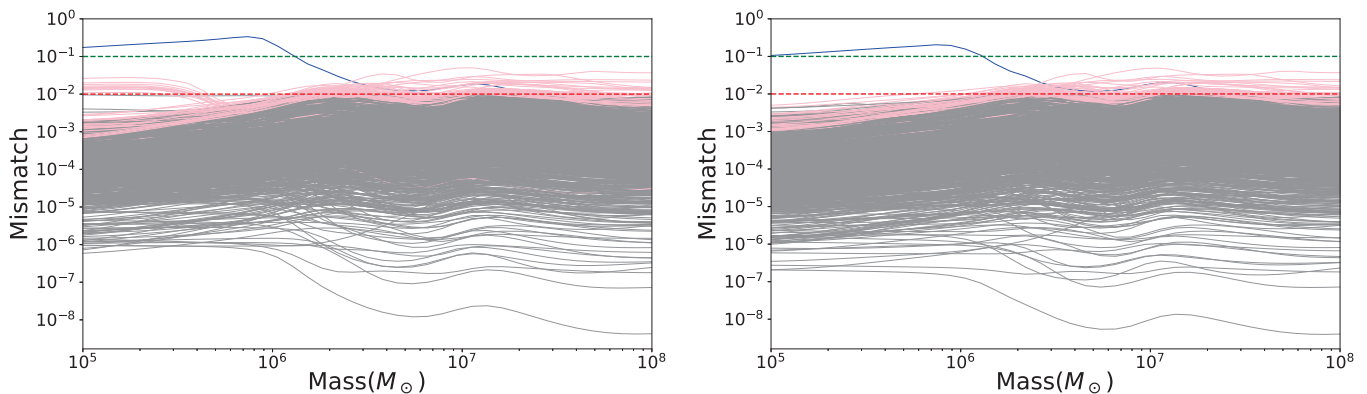


FIG. 6: Similar to Fig. 4 but with $f_{\text{low}} = \max(10^{-5}, 1.2f_{\text{min}})$ Hz (left panel) and $f_{\text{low}} = \max(10^{-5}, 1.5f_{\text{min}})$ Hz (right panel) instead of $f_{\text{low}} = \max(10^{-5}, f_{\text{min}})$ Hz. Like Fig. 5, we again use LISA as the example.

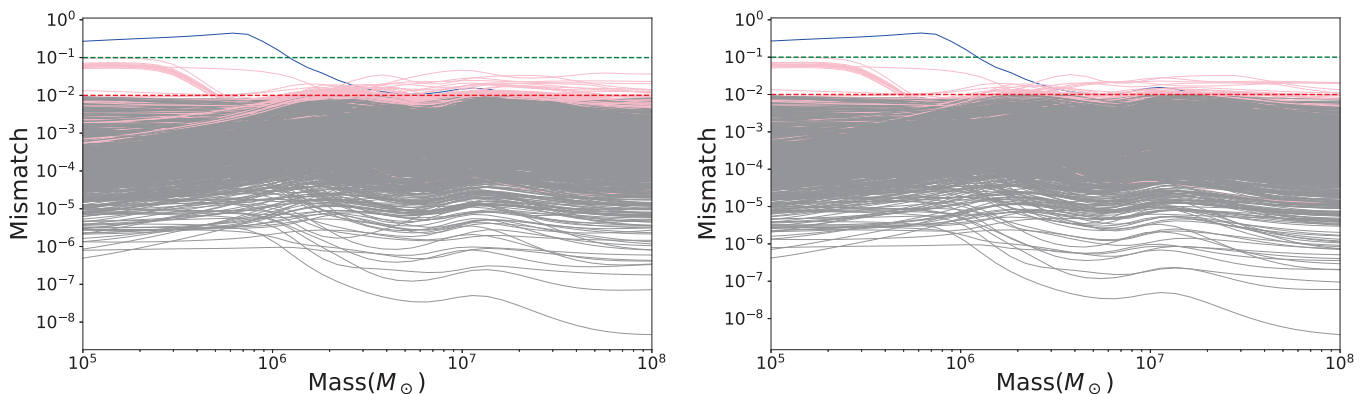


FIG. 7: Similar to Fig. 4 but with $f_{\text{up}} = \min(1, 0.8f_{\text{max}})$ Hz (left panel) and $f_{\text{up}} = \min(1, 0.5f_{\text{max}})$ Hz (right panel) instead of $f_{\text{up}} = \min(1, f_{\text{max}})$ Hz. Like Fig. 5, we again use LISA as the example.

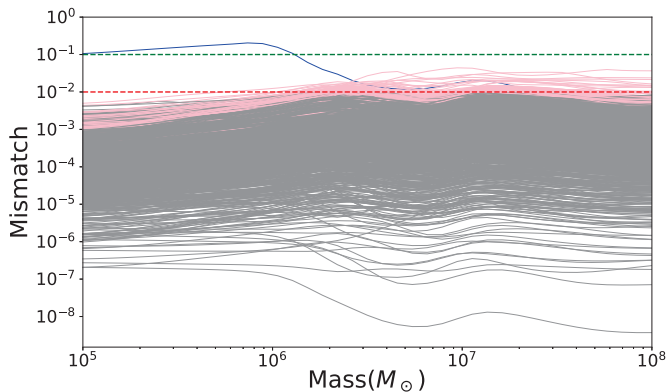


FIG. 8: Similar to Fig. 4 but with $f_{\text{low}} = \max(10^{-5}, 1.5f_{\text{min}})$ Hz and $f_{\text{up}} = \min(1, 0.8f_{\text{max}})$ Hz frequency choice instead of (36) and (37). Like Fig. 5, we again use LISA as the example.

clear unphysical oscillation near the low frequency f_{min} . In order to check the influence of such frequency range

choice, we have also considered

$$f_{\text{low}} = \max(10^{-5}, 1.2f_{\text{min}}), \quad (40)$$

$$f_{\text{up}} = \min(1, f_{\text{max}}), \quad (41)$$

and

$$f_{\text{low}} = \max(10^{-5}, 1.5f_{\text{min}}), \quad (42)$$

$$f_{\text{up}} = \min(1, f_{\text{max}}). \quad (43)$$

Similar to Fig. 5, we once again use LISA as example and plot the results in Fig. 6 for these two frequency range choices. As ones expected, when we consider shorter inspiral part, the waveform accuracy becomes higher. So we can see several lines above 10^{-2} in the left panel of Fig. 6 fall down below 10^{-2} in the right panel.

Regarding to high frequency side, we check how the cutting frequency affects the waveform accuracy. For comparison we have compared the results plotted in Fig. 4 to frequency choices

$$f_{\text{low}} = \max(10^{-5}, f_{\text{min}}), \quad (44)$$

$$f_{\text{up}} = \min(1, 0.8f_{\text{max}}), \quad (45)$$

and

$$f_{\text{low}} = \max(10^{-5}, f_{\text{min}}), \quad (46)$$

$$f_{\text{up}} = \min(1, 0.5f_{\text{max}}). \quad (47)$$

The result is shown in Fig. 7. As ones expected, the high frequency side affects large black hole mass systems more. But in all, the influence is small.

And more we have also considered conservative frequency range choice on both low and high frequency side

$$f_{\text{low}} = \max(10^{-5}, 1.5f_{\text{min}}), \quad (48)$$

$$f_{\text{up}} = \min(1, 0.8f_{\text{max}}). \quad (49)$$

The result is plotted in Fig. 8. In a short summary, the different frequency choices roughly result in similar waveform accuracy.

IV. SUMMARY AND CONCLUSION

One of the most challenging and fascinating problems in gravitational physics is to understand the dynamics of binary black hole mergers in the strong-field regime. In this regime, the components of the binary move at relativistic speeds and the spacetime curvature becomes highly nonlinear, making analytical approximations inadequate. The only reliable way to obtain precise solutions to Einstein's field equations in this regime is to use numerical relativity, which involves solving the full nonlinear equations on high-performance computers. This breakthrough was achieved in 2005 after decades of efforts [22].

Numerical relativity simulations of binary black hole mergers are essential for modeling the gravitational wave signals emitted by these systems during their late inspiral, merger, and ringdown phases. These signals are used to infer the properties of the source systems and to test general relativity in extreme conditions. All binary black hole detections made by LIGO and Virgo have been analyzed using waveform models that incorporate numerical relativity data. The most prominent examples of these models are the effective-one-body and phenomenological waveform models. Numerical relativity also plays a key role in validating these models and testing their accuracy and robustness. Moreover, numerical relativity waveforms can be directly used for parameter estimation, template bank construction, and waveform family

development without intermediate analytical steps, using techniques such as reduced order modeling.

Several coordinated efforts have been undertaken to produce numerical relativity simulations of binary black hole mergers for gravitational wave applications. These include the Numerical Injection Analysis (NINJA) project [51], the collaboration between Numerical Relativity and Analytical Relativity (NRAR), and the waveform catalogs released by the SXS collaboration and Georgia Tech.

In this work, we use numerical simulations of binary black hole mergers performed by the SXS Collaboration using the Spectral Einstein Code (SpEC). The SXS catalog has been used to construct SEOBNRE waveform model [28–31] and other waveform models. The accuracy of numerical relativity waveform is very important to gravitational wave astronomy study.

In previous works, the accuracy issue of numerical relativity waveform has been well studied for ground based detectors. In the current paper, we focus on space-based detectors. We have systematically investigated the effect of the waveform frequency range, the detector sensitivity detail, the BBH's black hole mass and others on the waveform accuracy issue.

Each waveform of SXS catalog has been investigated. Special attention is paid to matching factor calculation between highest and second highest resolution used in the numerical simulations. Our calculation results indicate that the numerical relativity waveforms are as accurate as 99% with respect to space-based detectors including LISA, Taiji and Tianqin. Such accuracy level is comparable to the one with respect to LIGO. If only the accuracy requirement for space-based detectors is similar to that of ground-based ones, the current numerical relativity waveforms are valid for waveform modelling.

Acknowledgments

This work was supported in part by the National Key Research and Development Program of China Grant No. 2021YFC2203001 and in part by the NSFC (No. 11920101003, No. 12021003 and No. 12005016). Z. Cao was supported by “the Interdiscipline Research Funds of Beijing Normal University” and CAS Project for Young Scientists in Basic Research YSBR-006.

-
- [1] The LIGO Scientific Collaboration, the Virgo Collaboration, the KAGRA Collaboration, R. Abbott, et al. GWTC-3: Compact Binary Coalescences Observed by LIGO and Virgo During the Second Part of the Third Observing Run. *arXiv e-prints*, page arXiv:2111.03606, November 2021.
- [2] The LIGO Scientific Collaboration, the Virgo Collabora-

tion, the KAGRA Collaboration, R. Abbott, et al. Open data from the third observing run of LIGO, Virgo, KAGRA and GEO. *arXiv e-prints*, page arXiv:2302.03676, February 2023.

- [3] M. Coleman Miller and Nicols Yunes. The new frontier of gravitational waves. *Nature*, 568(7753):469–476, Apr 2019.

- [4] Pau Amaro-Seoane et al. Astrophysics with the Laser Interferometer Space Antenna. *Living Reviews in Relativity*, 26(1):2, December 2023.
- [5] Piotr Jaranowski and Andrzej Królak. Gravitational-Wave Data Analysis. Formalism and Sample Applications: The Gaussian Case. *arXiv e-prints*, page arXiv:0711.1115, November 2007.
- [6] Andrzej Królak. Principles of Gravitational-Wave Data Analysis. In *Handbook of Gravitational Wave Astronomy*, page 43. 2021.
- [7] Lorenzo Speri, Nikolaos Karnesis, Arianna I. Renzini, and Jonathan R. Gair. A roadmap of gravitational wave data analysis. *Nature Astronomy*, 6:1356–1363, December 2022.
- [8] Nelson Christensen and Renate Meyer. Parameter estimation with gravitational waves. *Rev. Mod. Phys.*, 94:025001, Apr 2022.
- [9] Eric Chassande-Mottin, Eric Lebigot, Hugo Magaldi, Eve Chase, Archana Pai, Gayathri V, and Gabriele Vedovato. Wavelet graphs for the direct detection of gravitational waves. *arXiv e-prints*, page arXiv:1710.09256, October 2017.
- [10] P. Bacon, V. Gayathri, E. Chassande-Mottin, A. Pai, F. Salemi, and G. Vedovato. Driving unmodeled gravitational-wave transient searches using astrophysical information. *Phys. Rev. D*, 98:024028, Jul 2018.
- [11] Elena Cuoco, Jade Powell, Marco Cavaglià, Kendall Ackley, Michal Bejger, Chayan Chatterjee, Michael Coughlin, Scott Coughlin, Paul Easter, Reed Essick, Hunter Gabbard, Timothy Gebhard, Shaon Ghosh, Leila Haegel, Alberto Iess, David Keitel, Zsuzsa Marka, Szabolcs Marka, Filip Morawski, Tri Nguyen, Rich Ormiston, Michael Puerrer, Massimiliano Razzano, Kai Staats, Gabriele Vajente, and Daniel Williams. Enhancing Gravitational-Wave Science with Machine Learning. *arXiv e-prints*, page arXiv:2005.03745, May 2020.
- [12] Marlin B. Schäfer, Ondřej Zelenka, Alexander H. Nitz, He Wang, Shichao Wu, Zong-Kuan Guo, Zhoujian Cao, Zhixiang Ren, Paraskevi Nousi, Nikolaos Stergioulas, Panagiotis Iosif, Alexandra E. Koloniari, Anastasios Tefas, Nikolaos Passalis, Francesco Salemi, Gabriele Vedovato, Sergey Klimenko, Tanmaya Mishra, Bernd Brügmann, Elena Cuoco, E. A. Huerta, Chris Messenger, and Frank Ohme. First machine learning gravitational-wave search mock data challenge. *Phys. Rev. D*, 107(2):023021, January 2023.
- [13] He Wang, Shichao Wu, Zhoujian Cao, Xiaolin Liu, and Jian-Yang Zhu. Gravitational-wave signal recognition of ligo data by deep learning. *Phys. Rev. D*, 101:104003, May 2020.
- [14] Heming Xia, Lijing Shao, Junjie Zhao, and Zhoujian Cao. Improved deep learning techniques in gravitational-wave data analysis. *Phys. Rev. D*, 103:024040, Jan 2021.
- [15] CunLiang Ma, Wei Wang, He Wang, and Zhoujian Cao. Ensemble of deep convolutional neural networks for real-time gravitational wave signal recognition. *Phys. Rev. D*, 105:083013, Apr 2022.
- [16] Cunliang Ma, Wei Wang, He Wang, and Zhoujian Cao. Artificial intelligence model for gravitational wave search based on the waveform envelope. *Phys. Rev. D*, 107:063029, Mar 2023.
- [17] B. P. Abbott et al. Optically targeted search for gravitational waves emitted by core-collapse supernovae during the first and second observing runs of advanced ligo and advanced virgo. *Phys. Rev. D*, 101:084002, Apr 2020.
- [18] Frans Pretorius. Evolution of binary black-hole spacetimes. *Phys. Rev. Lett.*, 95:121101, Sep 2005.
- [19] M. Campanelli, C. O. Lousto, P. Marronetti, and Y. Zlochower. Accurate evolutions of orbiting black-hole binaries without excision. *Phys. Rev. Lett.*, 96:111101, Mar 2006.
- [20] John G. Baker, Joan Centrella, Dae-Il Choi, Michael Koppitz, and James van Meter. Gravitational-wave extraction from an inspiraling configuration of merging black holes. *Phys. Rev. Lett.*, 96:111102, Mar 2006.
- [21] Zhoujian Cao, Hwei-Jang Yo, and Jui-Ping Yu. Reinvestigation of moving punctured black holes with a new code. *Phys. Rev. D*, 78:124011, Dec 2008.
- [22] Tianyu Zhao, Zhoujian Cao, Chun-Yu Lin, and Hwei-Jang Yo. *Numerical Relativity for Gravitational Wave Source Modelling*, pages 1–30. Springer Singapore, Singapore, 2020.
- [23] Curt Cutler and Éanna E. Flanagan. Gravitational waves from merging compact binaries: How accurately can one extract the binary’s parameters from the inspiral waveform? *Phys. Rev. D*, 49:2658–2697, Mar 1994.
- [24] A. Buonanno and T. Damour. Effective one-body approach to general relativistic two-body dynamics. *Phys. Rev. D*, 59:084006, Mar 1999.
- [25] Alessandra Buonanno, Yi Pan, John G. Baker, Joan Centrella, Bernard J. Kelly, Sean T. McWilliams, and James R. van Meter. Approaching faithful templates for nonspinning binary black holes using the effective-one-body approach. *Phys. Rev. D*, 76:104049, Nov 2007.
- [26] Alejandro Bohé, Lijing Shao, Andrea Taracchini, Alessandra Buonanno, Stanislav Babak, Ian W. Harry, Ian Hinder, Serguei Ossokine, Michael Pürrer, Vivien Raymond, Tony Chu, Heather Fong, Prayush Kumar, Harald P. Pfeiffer, Michael Boyle, Daniel A. Hemberger, Lawrence E. Kidder, Geoffrey Lovelace, Mark A. Scheel, and Béla Szilágyi. Improved effective-one-body model of spinning, nonprecessing binary black holes for the era of gravitational-wave astrophysics with advanced detectors. *Phys. Rev. D*, 95:044028, Feb 2017.
- [27] Danilo Chiamarello and Alessandro Nagar. Faithful analytical effective-one-body waveform model for spin-aligned, moderately eccentric, coalescing black hole binaries. *Phys. Rev. D*, 101:101501, May 2020.
- [28] Zhoujian Cao and Wen-Biao Han. Waveform model for an eccentric binary black hole based on the effective-one-body-numerical-relativity formalism. *Phys. Rev. D*, 96:044028, Aug 2017.
- [29] Xiaolin Liu, Zhoujian Cao, and Lijing Shao. Validating the effective-one-body numerical-relativity waveform models for spin-aligned binary black holes along eccentric orbits. *Phys. Rev. D*, 101:044049, Feb 2020.
- [30] Xiaolin Liu, Zhoujian Cao, and Zong-Hong Zhu. A higher-multipole gravitational waveform model for an eccentric binary black holes based on the effective-one-body-numerical-relativity formalism. *Classical and Quantum Gravity*, 39(3):035009, February 2022.
- [31] Xiaolin Liu, Zhoujian Cao, and Lijing Shao. Upgraded waveform model of eccentric binary black hole based on effective-one-body-numerical-relativity for spin-aligned binary black holes. *International Journal of Modern Physics D*, 32:2350015, Feb 2023.
- [32] Geraint Pratten, Sascha Husa, Cecilio García-Quirós, Marta Colleoni, Antoni Ramos-Buades, Héctor Estellés,

- and Rafel Jaume. Setting the cornerstone for a family of models for gravitational waves from compact binaries: The dominant harmonic for nonprecessing quasicircular black holes. *Phys. Rev. D*, 102(6):064001, September 2020.
- [33] Cecilio García-Quirós, Marta Colleoni, Sascha Husa, Héctor Estellés, Geraint Pratten, Antoni Ramos-Buades, Maite Mateu-Lucena, and Rafel Jaume. Multimode frequency-domain model for the gravitational wave signal from nonprecessing black-hole binaries. *Phys. Rev. D*, 102:064002, Sep 2020.
- [34] Jonathan Blackman, Scott E. Field, Mark A. Scheel, Chad R. Galley, Christian D. Ott, Michael Boyle, Lawrence E. Kidder, Harald P. Pfeiffer, and Béla Szilágyi. Numerical relativity waveform surrogate model for generically precessing binary black hole mergers. *Phys. Rev. D*, 96:024058, Jul 2017.
- [35] Vijay Varma, Scott E. Field, Mark A. Scheel, Jonathan Blackman, Davide Gerosa, Leo C. Stein, Lawrence E. Kidder, and Harald P. Pfeiffer. Surrogate models for precessing binary black hole simulations with unequal masses. *Phys. Rev. Res.*, 1:033015, Oct 2019.
- [36] Tousif Islam, Vijay Varma, Jackie Lodman, Scott E. Field, Gaurav Khanna, Mark A. Scheel, Harald P. Pfeiffer, Davide Gerosa, and Lawrence E. Kidder. Eccentric binary black hole surrogate models for the gravitational waveform and remnant properties: Comparable mass, nonspinning case. *Phys. Rev. D*, 103:064022, Mar 2021.
- [37] Michael Boyle, Daniel Hemberger, Dante A. B. Iozzo, Geoffrey Lovelace, Serguei Ossokine, Harald P. Pfeiffer, Mark A. Scheel, Leo C. Stein, Charles J. Woodford, Aaron B. Zimmerman, Nousha Afshari, Kevin Barkett, Jonathan Blackman, Katerina Chatziioannou, Tony Chu, Nicholas Demos, Nils Deppe, Scott E. Field, Nils L. Fischer, Evan Foley, Heather Fong, Alyssa Garcia, Matthew Giesler, Francois Hebert, Ian Hinder, Reza Katebi, Haroon Khan, Lawrence E. Kidder, Prayush Kumar, Kevin Kuper, Halston Lim, Maria Okounkova, Teresita Ramirez, Samuel Rodriguez, Hannes R. Rüter, Patricia Schmidt, Bela Szilagyí, Saul A. Teukolsky, Vijay Varma, and Marissa Walker. The SXS collaboration catalog of binary black hole simulations. *Classical and Quantum Gravity*, 36(19):195006, October 2019.
- [38] LVK collaboration. Pycbc software. <https://pycbc.org/>.
- [39] Caltech-Cornell-CITA. binary black hole simulation results. <http://www.black-holes.org/waveforms>.
- [40] Tony Chu, Heather Fong, Prayush Kumar, Harald P Pfeiffer, Michael Boyle, Daniel A Hemberger, Lawrence E Kidder, Mark A Scheel, and Bela Szilagyí. On the accuracy and precision of numerical waveforms: Effect of waveform extraction methodology. *Classical and Quantum Gravity*, 33(16):165001, 2016.
- [41] DJA McKechnan, C Robinson, and Bangalore Suryanarayana Sathyaprakash. A tapering window for time-domain templates and simulated signals in the detection of gravitational waves from coalescing compact binaries. *Classical and Quantum Gravity*, 27(8):084020, 2010.
- [42] D Shoemaker (LIGO Scientific Collaboration). 2010 advanced ligo anticipated sensitivity curves ligo document t0900288-v3. URL <https://dcc.ligo.org/cgi-bin/DocDB/ShowDocument?docid=2974>, 2010.
- [43] M. Armano et al. Charge-induced force noise on free-falling test masses: Results from lisa pathfinder. *Phys. Rev. Lett.*, 118:171101, Apr 2017.
- [44] Wen-Hong Ruan, Chang Liu, Zong-Kuan Guo, Yue-Liang Wu, and Rong-Gen Cai. The lisa-taiji network. *Nature Astronomy*, 4(2):108–109, Feb 2020.
- [45] Jun Luo, Li-Sheng Chen, Hui-Zong Duan, Yun-Gui Gong, Shoucun Hu, Jianghui Ji, Qi Liu, Jianwei Mei, Vadim Milyukov, Mikhail Sazhin, et al. Tianqin: a spaceborne gravitational wave detector. *Classical and Quantum Gravity*, 33(3):035010, 2016.
- [46] Jun Luo, Yan-Zheng Bai, Lin Cai, Bin Cao, Wei-Ming Chen, Yu Chen, De-Cong Cheng, Yan-Wei Ding, Hui-Zong Duan, Xingyu Gou, Chao-Zheng Gu, De-Feng Gu, Zi-Qi He, Shuang Hu, Yuexin Hu, Xiang-Qing Huang, Qinghua Jiang, Yuan-Ze Jiang, Hong-Gang Li, Hong-Yin Li, Jia Li, Ming Li, Zhu Li, Zhu-Xi Li, Yu-Rong Liang, Fang-Jie Liao, Yan-Chong Liu, Li Liu, Pei-Bo Liu, Xuhui Liu, Yuan Liu, Xiong-Fei Lu, Yan Luo, Jianwei Mei, Min Ming, Shao-Bo Qu, Ding-Yin Tan, Mi Tang, Liang-Cheng Tu, Cheng-Rui Wang, Fengbin Wang, Guan-Fang Wang, Jian Wang, Lijiao Wang, Xudong Wang, Ran Wei, Shu-Chao Wu, Chun-Yu Xiao, Meng-Zhe Xie, Xiao-Shi Xu, Liang Yang, Ming-Lin Yang, Shan-Qing Yang, Hsien-Chi Yeh, Jian-Bo Yu, Lihua Zhang, Meng-Hao Zhao, and Ze-Bing Zhou. The first round result from the TianQin-1 satellite. *Classical and Quantum Gravity*, 37(18):185013, aug 2020.
- [47] Alexandre Toubiana, Sylvain Marsat, Stanislav Babak, John Baker, and Tito Dal Canton. Parameter estimation of stellar-mass black hole binaries with lisa. *Phys. Rev. D*, 102:124037, Dec 2020.
- [48] Travis Robson, Neil J Cornish, and Chang Liu. The construction and use of LISA sensitivity curves. *Classical and Quantum Gravity*, 36(10):105011, apr 2019.
- [49] Wen-Hong Ruan, Zong-Kuan Guo, Rong-Gen Cai, and Yuan-Zhong Zhang. Taiji program: Gravitational-wave sources. *International Journal of Modern Physics A*, 35(17):2050075, June 2020.
- [50] Neil Cornish and Travis Robson. Galactic binary science with the new lisa design. *Journal of Physics: Conference Series*, 840(1):012024, may 2017.
- [51] J. Aasi et al. The NINJA-2 project: detecting and characterizing gravitational waveforms modelled using numerical binary black hole simulations. *Classical and Quantum Gravity*, 31(11):115004, June 2014.